PTEP

Prog. Theor. Exp. Phys. **2016**, 093D01 (19 pages)
DOI: 10.1093/ptep/ptw125

General transformation of α cluster model wave function to *jj*-coupling shell model in various $4N$ nuclei

N. Itagaki[1,*], H. Matsuno[2], and T. Suhara[3]

[1]*Yukawa Institute for Theoretical Physics, Kyoto University, Kitashirakawa Oiwake-Cho, Kyoto 606-8502, Japan*
[2]*Department of Physics, Kyoto University, Kitashirakawa Oiwake-Cho, Kyoto 606-8502, Japan*
[3]*Matsue College of Technology, Matsue, Shimane 690-8518, Japan*
[*]E-mail: itagaki@yukawa.kyoto-u.ac.jp

Received June 16, 2016; Revised August 1, 2016; Accepted August 9, 2016; Published September 17, 2016

The antisymmetrized quasi-cluster model (AQCM) is a method to describe transitions from the α cluster wave functions to *jj*-coupling shell model wave functions. In this model, the cluster–shell transition is characterized by only two parameters: R representing the distance between α clusters and Λ describing the breaking of α clusters. The contribution of the spin–orbit interaction, very important in the *jj*-coupling shell model, can be taken into account starting with the α cluster model wave function. In this article we show the generality of AQCM by extending the application to heavier regions: various $4N$ nuclei from ^{4}He to ^{100}Sn. The characteristic magic numbers of the *jj*-coupling shell model, 28 and 50, are described starting with the α cluster model. The competition of two different configurations is discussed in ^{20}Ne (^{16}O + one quasi-cluster and ^{12}C + two quasi-clusters) and ^{28}Si (pentagon shape of five quasi-clusters and ^{12}C+^{16}O). Also, we compare the energy curves for the α+^{40}Ca cluster configuration calculated with and without the α breaking effect in ^{44}Ti.

Subject Index D11

1. Introduction

General description of shell and cluster structures is a dream of nuclear structure physics. Describing cluster states starting with shell models, including modern *ab initio* ones, is a big challenge of computational nuclear science [1–3]. In general, we need huge model space in order to describe spatially correlating nucleons located at some place with some distance from the origin, when the single particle wave function is expanded with respect to the origin [4,5]. On the other hand, if we start with the cluster model, we can easily describe cluster states with much less computational effort, but the contribution of non-central interactions, very important in nuclear structure [6,7], vanishes if we assume simple $(0s)^4$ configuration at some localized point for each α cluster. The real systems have both natures of shell and cluster structures, and quantum mechanical mixing of these two plays a crucial role in many cases [8–10], thus it is quite intriguing to establish a unified description for the nuclear structure. Our strategy is to start with the cluster model side, contrary to standard approaches that start with the shell model side, and try to extend the model space to include shell correlations, particularly for the contribution of the spin–orbit interaction.

As is well known, there is a certain overlap between the shell and cluster model spaces. When we take zero limit for the relative distance between clusters, the model space coincides with the lowest

shell model configuration owing to the antisymmetrization effect. This is called the Elliot SU(3) limit [11,12]. For instance, if we put four α particles in the form of a tetrahedron and take the zero limit for the relative α–α distances, the wave function coincides with the closed shell configuration of the p-shell. In this way, for $N = Z$ nuclei with magic numbers of a three-dimensional harmonic oscillator, cluster model wave functions can describe the doubly closed shell configurations of major shells. Here both spin–orbit-favored (j-upper) and -unfavored (j-lower) single particle orbits are filled and the contribution of the spin–orbit interaction cancels. However, it is necessary to break α clusters to take into account the spin–orbit contribution, if only spin–orbit-favored orbits of the last major shell are occupied. This is crucial for nuclei corresponding to the subclosure of the major shells. In addition, the "real" magic numbers of nuclear systems (beyond 20) indeed appear as a result of strong spin–orbit interaction, which is different from those corresponding to the closed shell configurations of three-dimensional harmonic oscillators.

To overcome this difficulty of the cluster model, we proposed the antisymmetrized quasi-cluster model (AQCM) [9,10,13–16], which enables us to describe the jj-coupling shell model states with the spin–orbit contribution starting with the cluster model wave function. In the AQCM, the transition from the cluster- to shell-model structure can be described by only two parameters: R representing the distance between α clusters, and Λ which characterizes the transition of α cluster(s) to quasi-cluster(s) and quantifies the role of the spin–orbit interaction. In Ref. [9], we have shown that the AQCM wave function in the limit of $R \to 0$ and $\Lambda = 1$ corresponds to the $(s_{1/2})^4(p_{3/2})^8$ closed shell configuration of ^{12}C, and the strong attractive contribution of the spin–orbit interaction can be taken into account. The optimal AQCM ground state of ^{12}C is an intermediate state between the three-α cluster state and the shell model state with the $p_{3/2}$ subshell closure configuration. From a comparison with the antisymmetrized molecular dynamics (AMD) model, where all nucleons are treated independently, we found that the AQCM result is consistent with the AMD result (the overlap is about 99%). This result is quite surprising, since the number of degrees of freedom in the AQCM trial wave function is significantly fewer than that in the AMD. In AMD, the Gaussian center parameters of all the nucleons are treated independently, and the number of degrees of freedom for the spatial part is 3 (three dimensions) $\times$ 2 (complex number) $\times$ A (number of nucleons), which is equal to $6A$, and they are variationally determined. In our model, we have only two control parameters, R and Λ. Nevertheless, these two approaches give similar results for ^{12}C.

The purpose of the present work is to show the general applicability of the AQCM framework in heavier regions. In this article, we apply AQCM to various $4N$ nuclei from ^{4}He to ^{100}Sn, where characteristic magic numbers for the jj-coupling shell model, 28 and 50, which are different from those of a three-dimensional harmonic oscillator, are included. We show that starting with the cluster model wave functions, we can generate jj-coupling shell model wave functions with the spin–orbit contribution. The competition of two different configurations is discussed in ^{20}Ne (^{16}O + one quasi-cluster and ^{12}C + two quasi-clusters) and ^{28}Si (pentagon shape of five quasi-clusters and ^{12}C+^{16}O). We also compare the energy curves for the α+^{40}Ca cluster configuration calculated with and without the α breaking effect in ^{44}Ti.

2. The model

In this section, we describe the AQCM wave function in this work.

2.1. *Single particle wave function (Brink model)*

In conventional α cluster models, the single particle wave function has a Gaussian shape [17],

$$\phi_i = \left(\frac{2\nu}{\pi}\right)^{\frac{3}{4}} \exp\left[-\nu\left(\vec{r}_i - \vec{R}_i\right)^2\right]\eta_i, \tag{1}$$

where η_i represents the spin–isospin part of the wave function, and $\vec{R}_i$ is a real parameter representing the center of a Gaussian wave function for the ith particle. In this Brink–Bloch wave function, four nucleons in one α cluster share a common $\vec{R}_i$ value. Hence, the contribution of the spin–orbit interaction vanishes.

2.2. *Single particle wave function in the AQCM*

In the AQCM, α clusters are changed into quasi-clusters. For nucleons in a quasi-cluster, the single particle wave function is described by a Gaussian wave packet, and the center of this packet $\vec{\zeta}_i$ is a complex parameter,

$$\psi_i = \left(\frac{2\nu}{\pi}\right)^{\frac{3}{4}} \exp\left[-\nu\left(\vec{r}_i - \vec{\zeta}_i\right)^2\right]\chi_i\tau_i, \tag{2}$$

where χ_i and τ_i represent the spin and isospin part of the ith single particle wave function, respectively. The spin orientation is governed by the parameters $\xi_{i\uparrow}$ and $\xi_{i\downarrow}$, which are in general complex parameters, while the isospin part is fixed to be "up" (proton) or "down" (neutron):

$$\chi_i = \xi_{i\uparrow}|\uparrow\rangle + \xi_{i\downarrow}|\downarrow\rangle, \tag{3}$$

$$\tau_i = |p\rangle \text{ or } |n\rangle. \tag{4}$$

The center of the packet $\vec{\zeta}_i$ has the form

$$\vec{\zeta}_i = \vec{R}_i + i\Lambda\vec{e}_i^{\,\text{spin}} \times \vec{R}_i, \tag{5}$$

where $\vec{e}_i^{\,\text{spin}}$ is a unit vector for the intrinsic-spin orientation, and Λ is a real control parameter describing the dissolution of the α cluster. As one can see immediately, the $\Lambda = 0$ AQCM wave function, which has no imaginary part, is the same as the conventional Brink–Bloch wave function. The AQCM wave function corresponds to a jj-coupling shell model wave function, such as a subshell closure configuration, when $\Lambda = 1$ and $\vec{R}_i \to 0$. The positive and negative Λ values correspond to the transformation to j-upper and j-lower orbits of the jj-coupling shell model, where the spin–orbit interaction acts attractively or repulsively. The mathematical explanation for it is summarized in Ref. [9]. For the width parameter, we use the value of $b = 1.46$ fm, $\nu = 1/2b^2$.

2.3. *AQCM wave function of the total system*

The wave function of the total system Ψ is the antisymmetrized product of these single particle wave functions:

$$\Psi = \mathcal{A}\{\psi_1\psi_2\psi_3\cdots\cdot\psi_A\}. \tag{6}$$

The projections onto parity and angular momentum eigenstates can be performed by introducing the projection operators P^J_{MK} and P^π, and these are performed numerically in the actual calculation.

2.4. Superposition of different configurations

Based on the generator coordinate method (GCM), the superposition of different AQCM wave functions is possible:

$$\Phi = \sum_i c_i P^J_{MK} P^\pi \Psi_i. \tag{7}$$

Here, $\{\Psi_i\}$ is a set of AQCM wave functions with different values of the R and Λ parameters, and the coefficients for the linear combination $\{c_i\}$ are obtained by solving the Hill–Wheeler equation [17],

$$\{\langle P^J_{MK} P^\pi \Psi_i | \hat{H} | P^J_{MK} P^\pi \Psi_j \rangle - E \langle P^J_{MK} P^\pi \Psi_i | P^J_{MK} P^\pi \Psi_j \rangle\} c_j = 0, \tag{8}$$

where E stands for the energy eigenvalue. We obtain a set of coefficients for the linear combination $\{c_j\}$ for each eigenvalue of E. In general, superposition of states projected to different K quantum numbers is also possible.

For the simplest case, we regard R and Λ as generator coordinates and superpose AQCM wave functions with different R and Λ values. However, more complex superpositions of different cluster configurations can be performed rather easily. We superpose different configurations, ^{16}O + quasi-cluster and ^{12}C+α+α in ^{20}Ne (where both the *jj*-coupling shell model and three-α configurations for the ^{12}C part are mixed) and a pentagon shape of five quasi-clusters and ^{12}C+^{16}O in ^{28}Si.

3. General applications of AQCM for various 4N nuclei

In this section, we show how we transform the cluster wave function to the *jj*-coupling shell model one in various nuclei from ^{4}He to ^{100}Sn.

3.1. ^{4}He and ^{8}Be

The ^{4}He nucleus is a closed shell configuration of the lowest s shell in the shell model description, and this agrees with the simple α cluster model wave function.

In ^{8}Be, four additional nucleons occupy $p_{3/2}$ orbits in the *jj*-coupling shell model, and we describe it by starting with a wave function of two α clusters and transforming it. Suppose that in the intrinsic frame, two α clusters are set on the x-axis with the relative distance R. This is realized by giving Gaussian center parameters [$\vec{R}_i$ in Eq. (1)] in the following way: $\vec{R}_1 = \vec{R}_2 = \vec{R}_3 = \vec{R}_4 = -R\vec{e}_x/2$, and $\vec{R}_5 = \vec{R}_6 = \vec{R}_7 = \vec{R}_8 = R\vec{e}_x/2$, where $\vec{e}_x$ is a unit vector in the x direction. Here, $\vec{R}_1$ and $\vec{R}_5$ are parameters for proton spin-up, $\vec{R}_2$ and $\vec{R}_6$ are for proton spin-down, $\vec{R}_3$ and $\vec{R}_7$ are for neutron spin-up, and $\vec{R}_4$ and $\vec{R}_8$ are for neutron spin-down nucleons. Based on Eq. (5), we transform two α clusters to quasi-clusters. Gaussian center parameters for the four protons are given in this way:

$$\vec{\zeta}_1 = -R(\vec{e}_x + i\Lambda\vec{e}_y)/2, \tag{9}$$

$$\vec{\zeta}_2 = -R(\vec{e}_x - i\Lambda\vec{e}_y)/2 = \vec{\zeta}_1^*, \tag{10}$$

$$\vec{\zeta}_5 = R(\vec{e}_x + i\Lambda\vec{e}_y)/2 = -\vec{\zeta}_1, \tag{11}$$

$$\vec{\zeta}_6 = R(\vec{e}_x - i\Lambda\vec{e}_y)/2 = -\vec{\zeta}_1^*, \tag{12}$$

where $\vec{e}_x$ and $\vec{e}_y$ are unit vectors in the x and y direction, respectively, and these are the same for the neutron part, $\vec{\zeta}_3 = \vec{\zeta}_1$, $\vec{\zeta}_4 = \vec{\zeta}_2$, $\vec{\zeta}_7 = \vec{\zeta}_5$, and $\vec{\zeta}_8 = \vec{\zeta}_6$. When Λ is set to zero, the wave function consisting of two quasi-clusters agrees with that of two α clusters.

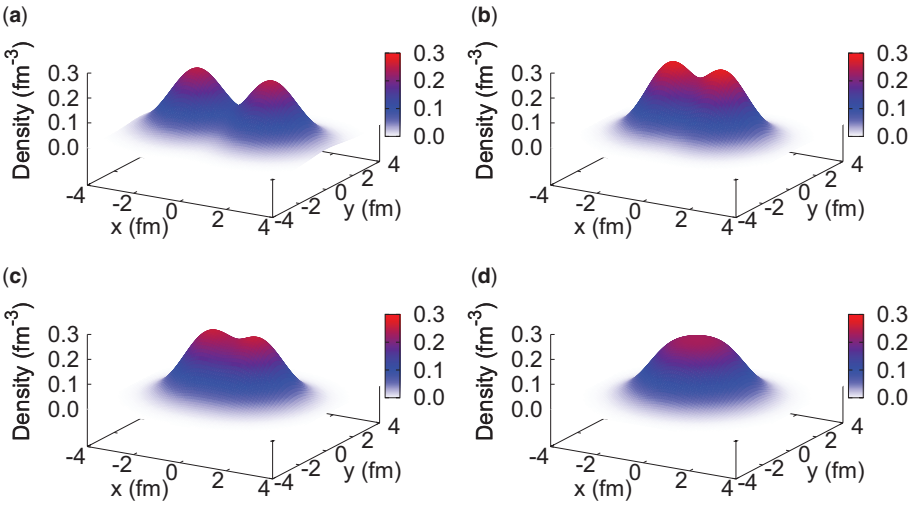

Fig. 1. (color online) Density plots of ^{8}Be on the $z = 0$ plane (xy-plane) as a function of R and Λ. (a) $R = 3$ fm, $\Lambda = 0$; (b) $R = 0.01$ fm, $\Lambda = 0$; (c) $R = 0.01$ fm, $\Lambda = 0.5$; and (d) $R = 0.01$ fm, $\Lambda = 1$. The integrated density is normalized to the number of nucleons.

Table 1. The expectation values of one-body spin–orbit operator $\sum_i \vec{l}_i \cdot \vec{s}_i$ in units of $\hbar^2$ (one-body ls) and principal quantum number (n) of ^{8}Be together with R (fm) and Λ values.

R (fm)	Λ	one-body ls	n
3.00	0.00	0.00	5.39
0.01	0.00	0.00	4.00
0.01	0.50	1.60	4.00
0.01	1.00	2.00	4.00

The density distributions of ^{8}Be as a function of R and Λ are shown in Fig. 1, where (a) $R = 3$ fm, $\Lambda = 0$; (b) $R = 0.01$ fm, $\Lambda = 0$; (c) $R = 0.01$ fm, $\Lambda = 0.5$; and (d) $R = 0.01$ fm, $\Lambda = 1$. In Fig. 1(a), we can recognize two distinct peaks due to the α clusters. The relative distance R is set to 3 fm, and α clusters are not dissolved ($\Lambda = 0$). These two peaks can still be clearly identified even if we take the zero limit for the relative distance R, owing to the antisymmetrization effect (Fig. 1(b) is the case of $R = 0.01$ fm). This is called the Elliot SU(3) state and is the first step in transforming the cluster model wave function to a shell model one. Then we transform α clusters to quasi clusters by changing Λ from zero to finite values; keeping $R = 0.01$ fm, the Λ value is increased to 0.5 in (c) and 1.0 in (d). Figure 1(c) is an intermediate state between the two-α cluster state and the shell model state, where the α cluster structure partially remains but it starts melting. In Fig. 1(d) we can see only one peak and the α cluster structure is washed out. Here the wave function is transformed to a jj-coupling shell model one.

The expectation values of the one-body spin–orbit operator in units of $\hbar^2$ (one-body ls) and principal quantum number of the harmonic oscillator (n) of ^{8}Be are listed in Table 1, together with R (fm) and Λ values. When $R = 3$ fm, the value of n is 5.39, and this value becomes 4.00 at $R = 0.01$ fm, which is the lowest possible value, where four of the nucleons are excited from the s shell to the p shell. The one-body spin–orbit operator ($\sum_i \vec{l}_i \cdot \vec{s}_i$) is a good tool to see this transition, since the expectation value becomes zero at $\Lambda = 0$, and this value becomes 2.00 at $\Lambda = 1$. This is because the four

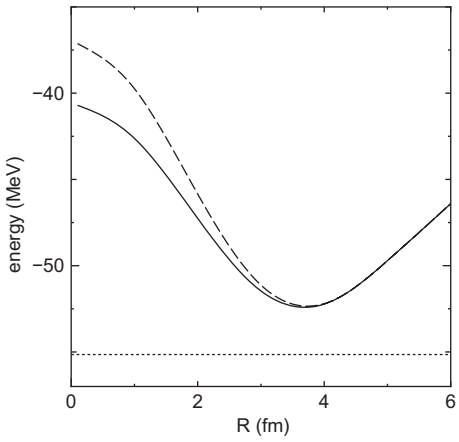

Fig. 2. The 0^+ energy curves of ^{8}Be. The dashed curve is for α–α as a function of parameter R representing the distance between two α's, and in the solid line, change into quasi-clusters is allowed. The optimal Λ value which gives the lowest energy is selected for each R value in the solid line. The dotted line at -55.14 MeV shows the threshold energy of two α clusters.

nucleons in the p_x shell are changed to $p_{3/2}$ orbits of the jj-coupling shell model. The expectation value for one nucleon in $p_{3/2}$ (in this case an eigenvalue) is

$$\langle \vec{l} \cdot \vec{s} \rangle = \{j(j+1) - l(l+1) - s(s+1)\}/2 = \{15/4 - 2 - 3/4\}/2 = 1/2,$$

and the value of 2.00 can be obtained by multiplying by 4, the number of nucleons in this orbit.

Next we show the 0^+ energy curve of α–α when α clusters are allowed to change into quasi-clusters. For the Hamiltonian, we use Volkov No. 2 [18] as an effective interaction for the central part, and the Majorana exchange parameter is set to $M = 0.60$, which is known to reproduce the scattering phase shift of two α clusters without breaking [19]. For the spin–orbit part, we use G3RS [20], which is a realistic interaction determined to reproduce the nucleon–nucleon scattering phase shift. We use the original strength of 600 MeV for the repulsive term and -1050 MeV for the attractive term. The angular momentum projection is numerically performed by rotating both the spins and Gaussian center parameters of the nucleons using Euler angles and integrating the wave function over these rotating angles. In Fig. 2, the dashed curve shows the 0^+ energy of α–α as a function of parameter R representing the distance between two α's. The spin–orbit interaction does not contribute since the α clusters are not broken. In the solid line, change into quasi-clusters is allowed, and the optimal Λ value which gives the lowest energy is selected for each R value. Although the spin–orbit interaction works in the solid line and this effect reduces the height of the repulsive core at $R = 0$ fm by about 3 MeV compared with the dashed line, the breaking of α clusters is rather limited in small-R regions. The energy curves of quasi-clusters are essentially not so different from the α clusters, which reproduce the scattering phase shift.

3.2. ^{12}C

The transformation of the three-α cluster wave function to the subclosure configuration of the $p_{3/2}$ shell in the jj-coupling shell model is discussed in Ref. [9] in detail. The basic idea is the following: one α cluster comprised of spin-up proton, spin-down proton, spin-up neutron, and spin-down neutron is placed on the x-axis; this is changed into a quasi-cluster as in the ^{8}Be case, and the second and

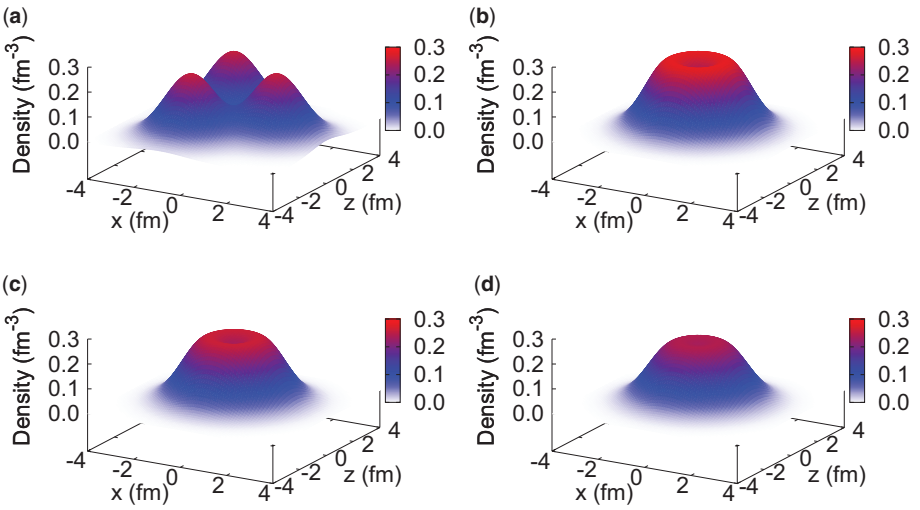

Fig. 3. (color online) The density plots of ^{12}C on the $y = 0$ plane (xz-plane) as a function of R and Λ. (a) $R = 3$ fm, $\Lambda = 0$; (b) $R = 0.01$ fm, $\Lambda = 0$; (c) $R = 0.01$ fm, $\Lambda = 0.5$; and (d) $R = 0.01$ fm, $\Lambda = 1$. The integrated density is normalized to the number of nucleons.

third quasi-clusters are introduced by rotating both spatial and spin parts of the first quasi-cluster around the y-axis by 120° and 240°, respectively.

The density distributions of ^{12}C on the $y = 0$ plane (xz-plane) as a function of R (distance between quasi-clusters) and Λ are shown in Fig. 3, where (a) $R = 3$ fm, $\Lambda = 0$; (b) $R = 0.01$ fm, $\Lambda = 0$; (c) $R = 0.01$ fm, $\Lambda = 0.5$; and (d) $R = 0.01$ fm, $\Lambda = 1$. In Fig. 3(a), we can recognize three distinct peaks due to the α clusters. The relative distance R is set to 3 fm and $\Lambda = 0$. These three peaks are changed into a donut shape if we take the zero limit for the relative distance R owing to the antisymmetrization effect (Fig. 3(b) is the case of R = 0.01 fm). Then we change Λ from zero to finite values; keeping $R = 0.01$ fm, the Λ value is increased to 0.5 in (c) and 1.0 in (d). We can see that the middle part of the donut is gradually filled, the α cluster structure is washed out, and the wave function is transformed to a jj-coupling shell model one.

It is quite instructive to compare the density distributions on the $y = 0$ plane (xz-plane) in Fig. 3 with the ones on the $z = 0$ plane (xy-plane). Figure 4 shows the density plot of ^{12}C on the $z = 0$ plane (xy-plane) with $R = 0.01$ fm and (a) $\Lambda = 0$, (b) $\Lambda = 1$. Here, Fig. 3(b) and Fig. 4(a) are the same case of $R = 0.01$ fm and $\Lambda = 0$, and the only difference is the axes of the figures; however, they look quite different. This means that even if inter-cluster distances are very small ($R = 0.01$ fm), the nucleus is deformed and not spherical in the Brink model description for ^{12}C. On the other hand, if we introduce Λ and transform α clusters to quasi-clusters, we can describe spherical ^{12}C corresponding to the subshell closure configuration; Fig. 3(d) and Fig. 4(b) are the same case of $R = 0.01$ fm and $\Lambda = 1$, and the distributions on the $y = 0$ plane (xz-plane) and on the $z = 0$ plane (xy-plane) are very similar. The nucleus has spherical symmetry.

The expectation values of one-body spin–orbit operator $\sum_i \vec{l}_i \cdot \vec{s}_i$ in units of $\hbar^2$ (one-body ls) and principal quantum number of the harmonic oscillator (n) of ^{12}C are listed in Table 2 together with R (fm) and Λ values. When $R = 3$ fm $n = 11.22$, and this value becomes 8.00 at $R = 0.01$ fm, which is the lowest possible value because eight nucleons are excited to the p shell. The one-body ls values are zero at $\Lambda = 0$, and this value becomes 4.00 at $\Lambda = 1$, interpreted as 0.5 (eigenvalue for a nucleon in $p_{3/2}$) times 8 (number of nucleons in this orbit).

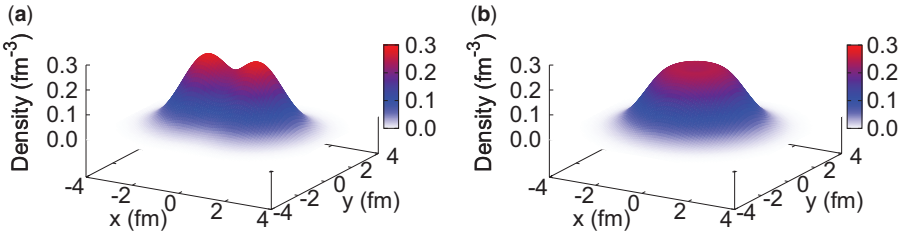

Fig. 4. (color online) The density plot of ^{12}C on the $z = 0$ plane (xy-plane) as a function of R and Λ. (a) $R = 0.01$ fm, $\Lambda = 0$; (b) $R = 0.01$ fm, $\Lambda = 1$. The integrated density is normalized to the number of nucleons.

Table 2. The expectation values of one-body spin–orbit operator $\sum_i \vec{l}_i \cdot \vec{s}_i$ in units of $\hbar^2$ (one-body ls) and principal quantum number of the harmonic oscillator (n) of ^{12}C together with R (fm) and Λ values.

R (fm)	Λ	one-body ls	n
3.00	0.00	0.00	11.22
0.01	0.00	0.00	8.00
0.01	0.50	3.33	8.00
0.01	1.00	4.00	8.00

Recently, D_{3h} symmetry has been intensively discussed in ^{12}C, which reflects the equilateral triangular shape of three α clusters [21]. The presence of the 3^- state at 9.6415 MeV is known, and for a long time this state has been considered as the band head of the $K^\pi = 3^-$ band, which reflects this symmetry. In addition, other members of this band, the 4^- and 5^- states, have been observed. In this article we have discussed that although the spin–orbit interaction plays a significant role that breaks the α clusters, there is a way to incorporate the spin–orbit effect without breaking the threefold symmetry of three-α clusters.

3.3. ^{16}O

For ^{16}O, which corresponds to the doubly closed shell of the shell model, it is not necessary to introduce quasi-clusters with Λ. If we take the zero limit for the relative distances of α clusters with a tetrahedron configuration, the wave function corresponds to the doubly closed shell configuration of the p shell of the jj-coupling shell model, where both $p_{3/2}$ and $p_{1/2}$ orbits are occupied.

3.4. ^{20}Ne and ^{24}Mg

There have been numerous works for ^{20}Ne based on the cluster models [22–25]. In addition to the ground $K^\pi = 0^+$ band, the negative parity band ($K^\pi = 0^-$) starting with the 1^- state at $E_x = 5.787726$ MeV has been observed, and existence of this "low-lying" negative parity band is strong evidence that the simple spherical mean field is broken. Recently the "container picture" has been proposed to describe the non-localization of the α cluster around ^{16}O [26]. However, according to the shell model, four nucleons perform independent particle motions around the ^{16}O core, which corresponds to the doubly closed shell of the p shell, and the spin–orbit interaction acts attractively on them. In our model, breaking of the α cluster can be easily done by introducing the Λ parameter for an α cluster outside the ^{16}O core. The change of the level structure as a function of the strength of

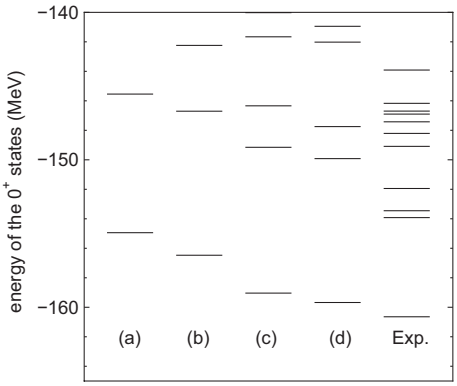

Fig. 5. The 0^+ energy levels of ^{20}Ne: (a) obtained with the ^{16}O+α model space; (b) obtained by coupling (a) with the basis states, where α is changed to a quasi-cluster; (c) ^{12}C+α+α states are coupled to (b), and the ^{12}C part is an equilateral triangular shape of three α clusters; (d) the breaking effect of α clusters in ^{12}C is taken into account by introducing the Λ parameter for ^{12}C. "Exp." stands for the observed 0^+ states.

the spin–orbit interaction within the ^{16}O + one quasi-cluster model space has already been discussed in Ref. [16].

Also, there have been discussions that the ^{12}C+α+α configuration plays an important role in the third 0^+ state. In Refs. [27–31], the ^{12}C+α+α cluster states have been coupled to ^{16}O+α; however, the ^{12}C part has been limited to three α clusters and the *jj*-coupling shell model state has not been introduced. Inclusion of all of these configurations can be done by applying AQCM, namely, the α cluster part of ^{16}O+α can be changed into a quasi-cluster and the ^{12}C cluster part of ^{12}C+α+α can be changed into a *jj*-coupling shell model wave function.

The Majorana exchange parameter of $M = 0.62$ for the Volkov interaction has been adopted to obtain a reasonable binding energy. For the spin–orbit part (G3RS interaction), we use the original strength of 600 MeV for the repulsive term and −1050 MeV for the attractive term. The size parameter of the Gaussian wave packet is chosen as $b = 1.6$ fm ($\nu = 1/2b^2$). Figure 5(a) shows the 0^+ energy levels obtained with the ^{16}O+α model space, where the distance parameter between two clusters has been chosen as $R = 1, 2, 3, 4, 5, 6$, and 7 fm. In this case, both the ground and second 0^+ states have ^{16}O+α configuration; however, it has been discussed that the observed second 0^+ state does not have large α clustering. Next we allow the breaking of the α cluster and (b) is the result, obtained by coupling (a) with the basis states with $\Lambda = 1/3, 2/3$, and 1. The α breaking components mix both in the ground and second 0^+ states; the energy of the ground state decreases by 2.5 MeV, and the wave function of the second 0^+ deviates from the higher nodal α–^{16}O cluster configuration. In Fig. 5(c), ^{12}C+α+α states are coupled with (b), where the ^{12}C part is described as an equilateral triangular shape of three α clusters with α–α distances of 0.5, 1, 1.5, 2, 2.5, and 3 fm. The positions of the other two α clusters are randomly assigned (the number of basis states for this configuration is 32). We can see that the energy of the third 0^+ state strongly decreases. Finally, the breaking effect of α clusters in ^{12}C is taken into account in Fig. 5(d) by introducing the Λ parameter for ^{12}C, and the energy of the third 0^+ state further decreases. Here again the positions of the other two α clusters are randomly assigned, and the number of basis states for this configuration is 40.

We can conclude that the energy of the third 0^+ is most affected by the inclusion of ^{12}C+α+α model space. However, the energies of the first and second 0^+ states also decrease and coupling of two different model spaces is found to be important (the excitation energy of the second 0^+ state is therefore almost constant in spite of enlarging the model spaces), and unfortunately, the excitation

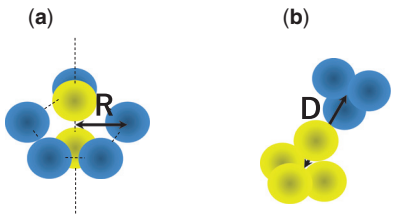

Fig. 6. (color online) Schematic figures for ^{28}Si. Spheres represent α clusters, and blue ones are changed into quasi-clusters. (a) Five quasi-cluster are placed in a pentagon shape on a plane at a distance R from the origin, and two α clusters are set on the vertical axis at $R/2$ and $-R/2$. (b) ^{12}C+^{16}O shape. The parameter D is set for the distance between ^{12}C and ^{16}O. ^{12}C consists of three quasi-clusters and ^{16}O consists of four α clusters with a tetrahedron shape.

energy of the third 0^+ state is still higher than experiment, since the binding energy of the ^{12}C cluster part is underestimated in the framework. This is related to a fundamental problem of the interactions in microscopic cluster models that the ^{12}C cluster becomes under-bound when ^{16}O is reproduced [32].

The *jj*-coupling shell model wave functions of ^{24}Mg are easily generated by adding one quasi-cluster to ^{20}Ne. A simple application can be found in Ref. [16].

3.5. ^{28}*Si*

For ^{28}Si, there are two ways to transform the α cluster wave function to the subclosure configuration of $d_{5/2}$ in the *jj*-coupling shell model. One configuration is a pentagon shape of five quasi-α clusters on the xz-plane with two α clusters placed on the y-axis [Fig. 6(a)]. Another configuration consists of a tetrahedron shape of four α clusters whose center of gravity is at the origin and a triangle shape of three quasi-α clusters on the xy-plane surrounding four α's [Fig. 6(b)]. For the former case, as schematically shown in Fig. 6(a), one α cluster comprised of spin-up proton, spin-down proton, spin-up neutron, and spin-down neutron is placed on the x-axis and this is changed into a quasi-cluster by giving Λ as in the ^{8}Be case, and the second, third, fourth, and fifth quasi-clusters are introduced by rotating both spatial and spin parts of the first quasi-cluster around the y-axis by 72°, 144°, 216°, and 288°, respectively. In addition, we place two α clusters on the y-axis. The latter configuration is the combination of ^{12}C and ^{16}O wave functions described in the previous subsection [Fig. 6(b)], and here the 12 nucleons of ^{12}C are excited to the *sd* shell due to the antisymmetrization effect. If we take the zero limit for the relative distances among α clusters and quasi-clusters, these two configurations become identical and give the lowest shell model configuration of $(s_{1/2})^4(p_{3/2})^8(p_{1/2})^4(d_{5/2})^{12}$ at $\Lambda = 1$.

The expectation value of the one-body spin–orbit operator $\sum_i \vec{l}_i \cdot \vec{s}_i$ for ^{28}Si is shown in Fig. 7 in units of $\hbar^2$. The five quasi-α clusters form a pentagon shape on the xz-plane as in Fig. 6(a) with the distance $R = 0.01$ fm, and Λ is changed from 0 to 1. The eigenvalue for the one-body spin–orbit operator is 1 for a nucleon in the $d_{5/2}$ orbit, and for ^{28}Si, the value should be 12 because of the 12 nucleons in $d_{5/2}$; this is achieved at $\Lambda = 1$.

The 0^+ energy curves of ^{28}Si as functions of the distance parameter R are shown in Fig. 8. Here, the Majorana exchange parameter of $M = 0.62325$ for the Volkov interaction has been adopted to obtain a reasonable binding energy. For the spin–orbit part (G3RS interaction), we use the original strength of 600 MeV for the repulsive term and -1050 MeV for the attractive term. The dashed line is the case of $\Lambda = 0$ for the quasi-clusters, which is equivalent to α clusters. For the solid line, the

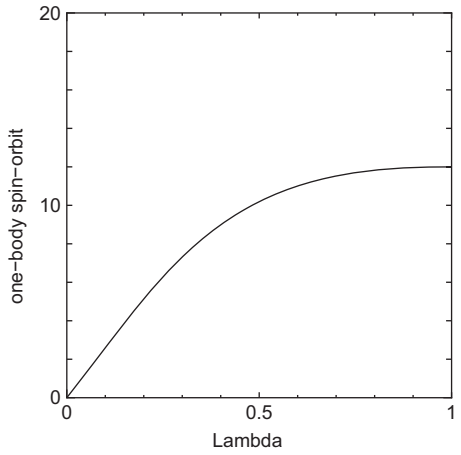

Fig. 7. The expectation value of the one-body spin–orbit operator ($\sum_i \vec{l}_i \cdot \vec{s}_i$) for ^{28}Si in units of $\hbar^2$. The five quasi-α clusters form a pentagon shape on the xz-plane with the distance $R = 0.01$ fm, and two α clusters are set on the y-axis at $R/2$ and $-R/2$ as in Fig. 6(a). The Λ value is changed from 0 to 1.

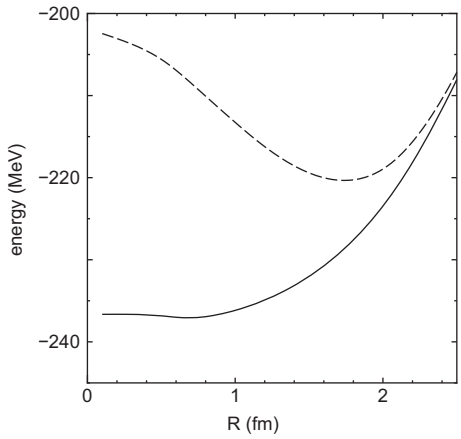

Fig. 8. The 0^+ energy curves of ^{28}Si with the pentagon shape as functions of the distance parameter R. Five quasi-clusters are placed with a pentagon shape at the distance of R from the origin and two α clusters are set on the vertical axis at $R/2$ and $-R/2$, as in Fig. 6(a). The dashed line is the case of $\Lambda = 0$ for the quasi-clusters, which is equivalent to α clusters, and for the solid line, the optimal Λ value giving the lowest energy is chosen for each R.

optimal Λ value giving the lowest energy is chosen for each R. At $R = 0.1$, the breaking effect of α clusters due to the spin–orbit interaction is quite large; the optimal Λ value giving the lowest energy is 0.31, and the energy difference of two lines is about 34 MeV. When R gets larger and becomes 2 fm, the energy of the solid line is higher than the lowest one by 10 MeV, and in this region, the breaking effect of α clusters is rather limited.

For the ^{12}C+^{16}O configuration, the 0^+ energy curves as functions of the distance parameter D between ^{12}C and ^{16}O are shown in Fig. 9. Here, ^{16}O consists of four α clusters with a distance of 0.1 fm between their centers of mass, whereas ^{12}C consists of three quasi-clusters whose distances should be slightly larger than the ^{16}O case, and now they are set to 0.2 fm as shown in Fig. 6(b). When Λ is small, three quasi-clusters form a triangular shape, and the ^{16}O is placed in a perpendicular direction to the plane of this triangle; however, three quasi-clusters are transformed into a spherical

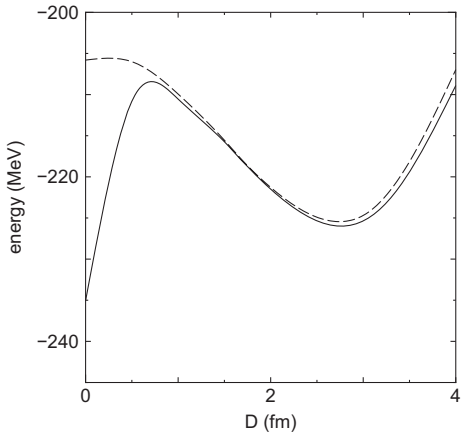

Fig. 9. The 0^+ energy curves of ^{28}Si with the ^{12}C+^{16}O shape as functions of the distance parameter D between ^{12}C and ^{16}O, as in Fig. 6(b). Here, ^{12}C consists of three quasi-clusters which have a distance of 0.2 fm between their centers of mass, and ^{16}O consists of four α clusters with a distance of 0.1 fm between their centers of mass. The dashed line is the case of $\Lambda = 0$ for the quasi-clusters, equivalent to α clusters, and the optimal Λ value giving the lowest energy is chosen for each D in the solid line.

density distribution with increasing Λ value. The dashed line is the case of $\Lambda = 0$ for the quasi-clusters, which is equivalent to α clusters, and for the solid line, the optimal Λ value giving the lowest energy is chosen for each D. When D is small, the breaking of α clusters is quite important due to the subclosure configuration of $d_{5/2}$, and the energy of the solid line (the optimal Λ giving the lowest energy is chosen) is about 30 MeV lower than the dashed line ($\Lambda = 0$). At D (^{12}C–^{16}O distance) = 0 fm, the selected Λ value in the solid line is 0.46. However, a local energy minimum point appears around $D = 3$ fm and the solid and dashed lines give almost equivalent energies around this region. Here, the ^{12}C (3α) + ^{16}O cluster configuration plays a dominant role.

In our previous study on ^{28}Si based on the seven-α model, the spin–orbit interaction was not taken into account, and the ground state was a prolate shape with the ^{12}C (3α) + ^{16}O configuration [33]. If we compare the lowest energy of the pentagon shape in Fig. 8 and the local minimum energy of ^{12}C (3α) + ^{16}O in Fig. 9, we can conclude that the spin–orbit interaction is shown to play a big role for the lowering of the pentagon shape, which is oblate.

Next, we mix these two configurations, the pentagon shape and ^{12}C+^{16}O. If we perform a GCM (generator coordinate method) calculation by superposing basis states on the energy curves of Figs. 8 and 9, the first 0^+ is obtained at -238.0 MeV and the second one is obtained at -226.5 MeV. The main component of the first one is the pentagon shape. This energy difference is much larger than the experimental value of 4.979928 MeV, and fine-tuning of the spin–orbit interaction is necessary; however, without the spin–orbit force, the energy of the ^{12}C+^{16}O configuration is lower than the pentagon shape, and this energy difference is really sensitive to the strength of the spin–orbit interaction.

3.6. ^{40}Ca

^{40}Ca corresponds to the doubly closed shell of the *sd* shells, and the cluster model and *jj*-coupling shell model give the same representation without introducing quasi-clusters with Λ. Starting with the α cluster model, this is achieved by taking the zero limit for the distance parameter R of ten α clusters; one α is centered at the origin (the yellow sphere in Fig. 10), six α's are on the x-, y-, and z-axes at $R\vec{e}_x$, $-R\vec{e}_x$, $R\vec{e}_y$, $-R\vec{e}_y$, $R\vec{e}_z$, $-R\vec{e}_z$ (the blue spheres in Fig. 10), and the last three α's are on the xy-, yz-, and xy-planes at $R(\vec{e}_x + \vec{e}_y)/\sqrt{2}$, $R(-\vec{e}_y + \vec{e}_z)/\sqrt{2}$, and $-R(\vec{e}_x + \vec{e}_z)/\sqrt{2}$ (the red

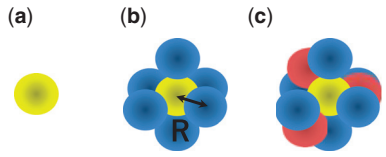

Fig. 10. (color online) Schematic figure for the ten α clusters for ^{40}Ca. (a) One α cluster at the origin. (b) Adding six α clusters on the x-, y-, and z-axes (two α clusters for each axis). (c) Adding three α clusters on the xy-, yz-, and xz-planes. R represents the distance between each α cluster and the origin.

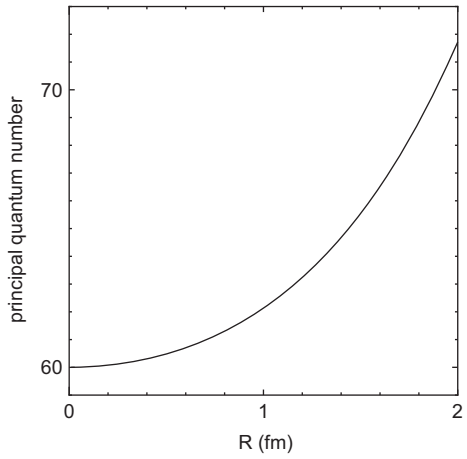

Fig. 11. The expectation value of the principal quantum number of the harmonic oscillator for ^{40}Ca as a function of the distance parameter R between each α cluster and the origin.

spheres in Fig. 10), where $\vec{e}_x$, $\vec{e}_y$, and $\vec{e}_z$ are unit vectors in the x, y, and z directions, respectively. Here, R represents not the relative distances of α clusters but the distance from the origin.

The expectation value of the principal quantum number n of the harmonic oscillator for ^{40}Ca is shown in Fig. 11 as a function of the distance parameter R (the distance between each α cluster and the origin). At $R = 0$ fm, the value converges to 60, reflecting the fact that the 12 nucleons are in the p shell and 24 nucleons are in the sd shell.

3.7. ^{44}Ti and ^{52}Fe

For ^{44}Ti, the ^{40}Ca+α cluster structure has been widely discussed in many theories and experiments [34–37]. Also, in ^{52}Fe, the possibility of a three-α structure around the ^{40}Ca has been suggested [38,39]. The transition from such α cluster states to the lowest jj-coupling shell model state can be easily discussed within the present AQCM approach.

The jj-coupling shell model wave functions of ^{44}Ti are easily generated by adding one quasi-cluster around the ^{40}Ca core. This is performed just by replacing the ^{16}O core in our analysis for ^{20}Ne and ^{24}Mg in Ref. [16] with the ^{40}Ca core introduced in the previous subsection. The expectation value of the one-body spin–orbit operator ($\sum_i \vec{l}_i \cdot \vec{s}_i$) for ^{44}Ti is shown in Fig. 12 in units of $\hbar^2$ (solid line). One quasi-cluster is placed on the x-axis with a distance of $R = 0.1$ fm from the ^{40}Ca core, and Λ is changed from 0 to 1 (R in Fig. 10 for the ^{40}Ca core part is set to 0.01 fm, smaller than the value for the quasi-cluster). The expectation value for the one-body spin–orbit operator (in this case the eigenvalue) is 3/2 for a nucleon in the $f_{7/2}$ orbit,

$$\langle \vec{l} \cdot \vec{s} \rangle = \{j(j+1) - l(l+1) - s(s+1)\}/2 = \{63/4 - 12 - 3/4\}/2 = 3/2,$$

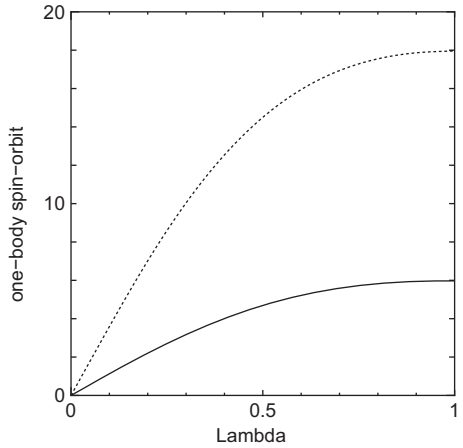

Fig. 12. The expectation value of the one-body spin–orbit operator ($\sum_i \vec{l}_i \cdot \vec{s}_i$) for ^{44}Ti in units of $\hbar^2$ (solid line). One quasi-cluster is placed on the x-axis at a distance of $R = 0.1$ fm from the ^{40}Ca core, and Λ is changed from 0 to 1. The value for ^{52}Fe is shown by the dotted line, and the distance parameter R for the three quasi-clusters is set to 0.25 fm. For the ^{40}Ca core part, R in Fig. 10 is set to 0.01 fm, smaller than the value for the quasi-cluster(s).

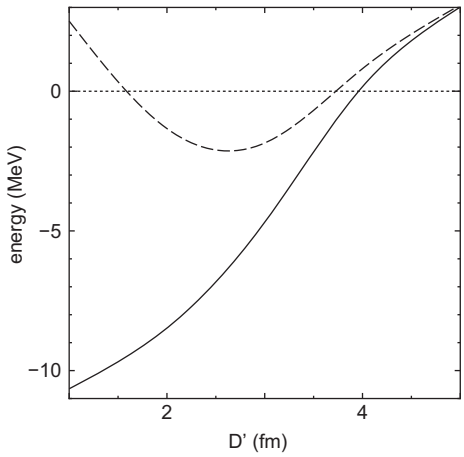

Fig. 13. The 0^+ energy curves of ^{44}Ti comprised of ^{40}Ca and one quasi-cluster as functions of the relative distance D'. The dashed line is the case of $\Lambda = 0$ for the quasi-cluster (^{40}Ca+α model), and for the solid line the optimal value of Λ giving the lowest energy is chosen for each D' value. The energies are measured from the ^{40}Ca+α threshold (dotted line).

and for ^{44}Ti, the value should be 6 because of four nucleons in $f_{7/2}$. In Fig. 12 (solid line), we can recognize that this situation is achieved at $\Lambda = 1$.

Next we show the energy curve of ^{44}Ti and discuss the cluster–shell competition. It has been known that we have to increase the value of the Majorana exchange parameter with increasing mass number, and here $M = 0.65$ has been adopted. This parameter gives a reasonable binding energy of one α cluster around ^{40}Ca before taking into account the α breaking effect. The 0^+ energy curves of ^{44}Ti comprised of ^{40}Ca and one quasi-cluster as functions of the relative distance D' between them are shown in Fig. 13. The value of R in Fig. 10 for the ^{40}Ca core is set to 0.1 fm. The dashed line is the case of $\Lambda = 0$ for the quasi-cluster, which is equivalent to an α cluster, and for the solid line, the optimal value of Λ giving the lowest energy is chosen for each D' value. The energies are measured from the ^{40}Ca+α threshold (dotted line). We can see a very large difference between these two curves,

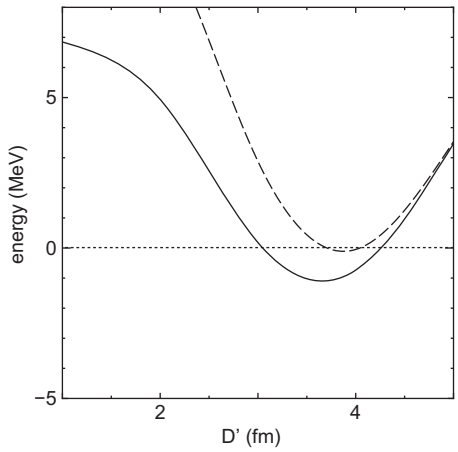

Fig. 14. The 1^- energy curves of ^{44}Ti comprised of ^{40}Ca and one quasi-cluster as functions of the relative distance D'. The dashed line is the case of $\Lambda = 0$ for the quasi-cluster (^{40}Ca+α model), and for the solid line the optimal value of Λ giving the lowest energy is chosen for each D' value. The energies are measured from the ^{40}Ca+α threshold (dotted line).

about 10 MeV around $D' = 1$ fm, because of the contribution of the spin–orbit interaction in the solid line, and the optimal Λ value giving the lowest energy here is 0.69. Although fine-tuning of the interaction is needed for precise spectroscopy, at the moment we can say that the effect of the spin–orbit interaction is quite large and that is clearly described by transforming α cluster states to the *jj*-coupling shell model. one.

On the other hand, the effect of α breaking is limited around the energy minimum point of the 1^- state, as shown in Fig. 14. The α clustering has been known to play an essential role for the lowering of the negative parity states, and the discovery of negative parity states and inversion doublet structure in the low-lying region of this nucleus were the keys to establishing the concept that the cluster structure is not limited to very light nuclei and is more general. We can see that the optimal energy is obtained around the distance parameter D' between quasi-cluster and ^{40}Ca of 3.5 fm and clustering is really important, where the decrease of the energy is limited to be about 1 MeV when breaking of α clusters to quasi-clusters is allowed, and the optimal Λ value giving the lowest energy is 0.08.

For ^{52}Fe, the *jj*-coupling wave function is easily prepared by placing our ^{12}C (three quasi-clusters) around the ^{40}Ca core introduced in the previous subsections. Here, 12 nucleons of ^{12}C are excited to the *pf* shell ($f_{7/2}$) due to the antisymmetrization effect. The details for changing three α clusters into three quasi-clusters are shown in Ref. [9], and here we just add the ^{40}Ca core introduced in the previous subsection in the center of the three quasi-clusters.

The expectation value of the one-body spin–orbit operator ($\sum_i \vec{l}_i \cdot \vec{s}_i$) for ^{52}Fe is shown in Fig. 12 in units of $\hbar^2$ (dotted line). The distance parameter for the three quasi-clusters is taken as $R = 0.25$ fm (R in Fig. 10 for the ^{40}Ca core part is set to 0.01 fm, smaller than the value for the quasi-clusters), and Λ is changed from 0 to 1. The eigenvalue for the one-body spin–orbit operator is 3/2 for a nucleon in the $f_{7/2}$ orbit, and for ^{52}Fe, the value should be 18 because of the 12 nucleons in $f_{7/2}$. In Fig. 12, this is achieved at $\Lambda = 1$.

3.8. ^{56}Ni and ^{100}Sn

With increasing mass number, the magic numbers of the *jj*-coupling shell model deviate from those of the three-dimensional harmonic oscillator. Using AQCM, we can transform wave functions of the

Brink model first to the three-dimensional harmonic oscillator (by taking the limit of $R \to 0$) and next to the *jj*-coupling shell model (by taking the limit of $\Lambda = 1$) for nuclei corresponding to magic numbers of 28 and 50.

For the magic number 28, the nucleus of ^{56}Ne is described by preparing four quasi-clusters around the ^{40}Ca core. Describing the closed-shell configuration of $(f_{7/2})^8$ can be achieved by placing four α clusters in the form of a tetrahedron and changing them to quasi-clusters. However, placing four α clusters on a two-dimensional plane and changing them to quasi-clusters is even simpler. When placing on a plane, note that it is necessary to place the in a trapezoidal shape. If we place them in the form of a square, two of the quasi-clusters are excited not to *pf* shell orbits but to *sdg* shell orbits due to the symmetry of the shape. This situation is explained in the following way. Suppose that two α clusters are set on the x-axis and the ^{40}Ca core stays at the origin. By taking linear combinations of the wave functions of nucleons in these α clusters, four nucleons occupy the *pf* shell orbits as expected; however, the other four nucleons are excited to the *sdg* shell orbits because of the orthogonal condition to the wave functions of the first four nucleons. The same thing happens for the nucleons placed on the y-axis. We can avoid this risk by placing them in a trapezoidal shape. For instance, one of the α clusters around the ^{40}Ca core is placed on the x-axis, where the imaginary parts of the Gaussian center parameters are given in the y direction and the spin is quantized in the z direction. The other α clusters are introduced by rotating both the spatial and spin parts of the first cluster about the y-axis by 90°, 210°, and 240°, respectively. The 16 nucleons in 4 quasi-clusters correspond to $f_{7/2}$ orbits at the limit of $R \to 0$ and $\Lambda = 1$.

The expectation value of the one-body spin–orbit operator $(\sum_i \vec{l}_i \cdot \vec{s}_i)$ for ^{56}Ni is shown in Fig. 15 in units of $\hbar^2$. The eigenvalue for the one-body spin–orbit operator is 3/2 for a nucleon in the $f_{7/2}$ orbit, and the value for ^{56}Ni becomes 24 because of the 16 nucleons in $f_{7/2}$ at $R \to 0$ and $\Lambda = 1$. In this way, the characteristic magic number of 28 in the *jj*-coupling shell model can be described starting with the Brink model.

For the magic number 50, we show the result for ^{100}Sn. At first we prepare an ^{80}Zr core by placing 20 α clusters in a similar way to ^{40}Ca (first we construct the ^{40}Ca core as in the previous subsections and add ten α clusters around it). The nucleus ^{80}Zr corresponds to the doubly closed shell configuration for the principal quantum number $N = 3$ in the three-dimensional harmonic oscillator.

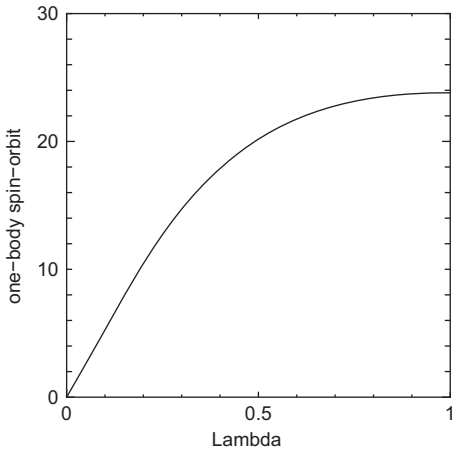

Fig. 15. The expectation value of the one-body spin–orbit operator $(\sum_i \vec{l}_i \cdot \vec{s}_i)$ for ^{56}Ni in units of $\hbar^2$. The Λ value is changed from 0 to 1.

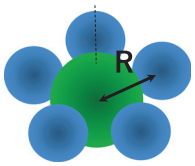

Fig. 16. (color online) Schematic figure for ^{100}Sn. The five blue spheres represent α clusters, which are changed into quasi-clusters. The big sphere in the middle represents the ^{80}Zr core described by 20 α clusters.

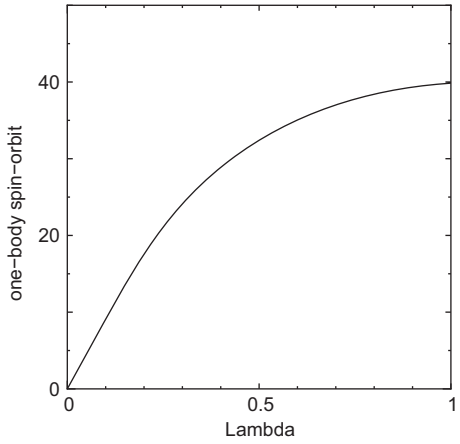

Fig. 17. The expectation value of the one-body spin–orbit operator $(\sum_i \vec{l}_i \cdot \vec{s}_i)$ for ^{100}Sn in units of $\hbar^2$. The Λ value is changed from 0 to 1.

For ^{100}Sn, the *jj*-coupling wave function is easily prepared by placing five α clusters around the ^{80}Zr core in a pentagon shape, as in Fig. 16. Here, 20 nucleons in α clusters are excited to the *sdg* shell due to the antisymmetrization effect. One of the α clusters around the ^{80}Zr core is placed on the x-axis, where the imaginary parts of the Gaussian center parameters are given in the y direction and the spin is quantized in the z direction. The other quasi-clusters are introduced by rotating both the spatial and spin parts of the first cluster about the y-axis by 72°, 144°, 216°, and 288°, respectively. These 20 nucleons correspond to $g_{9/2}$ orbits at the limit of $R \to 0$ and $\Lambda = 1$.

The expectation value of the one-body spin–orbit operator $(\sum_i \vec{l}_i \cdot \vec{s}_i)$ for ^{100}Sn is shown in Fig. 17 in units of $\hbar^2$. The distance parameter for the five quasi-clusters is taken as $R = 0.25$ fm, and Λ is changed from 0 to 1. The eigenvalue for the one-body spin–orbit operator is 2.0 for a nucleon in the $f_{9/2}$ orbit, and the value should be 40 because of 20 nucleons in $g_{9/2}$. In Fig. 17 this is achieved at $\Lambda = 1$.

4. Summary

We have shown that AQCM, which is a method to describe transitions from α cluster wave functions to the *jj*-coupling shell model wave functions, can be extended to heavier regions. In this model, this cluster–shell transition is characterized by only two parameters: R representing the distance between α clusters and Λ describing the breaking of α clusters. The contribution of the spin–orbit interaction, very important in the shell model, can be taken into account starting with the α cluster model wave functions. The *jj*-coupling shell model states are realized at the limit of $R \to 0$ and $\Lambda \to 1$. We have shown the generality of this model in various $4N$ nuclei from ^{4}He to ^{100}Sn,

including characteristic magic numbers of the *jj*-coupling shell model, 28 and 50, different from those of the three-dimensional harmonic oscillator.

For *sd* shell nuclei, we discussed, for instance in ^{28}Si, that there are two ways to transform the α cluster model wave function to the closed $d_{5/2}$ configuration of the *jj*-coupling wave function, which become identical at the limit of $R \to 0$ and $\Lambda \to 1$; however, a difference appears when the distance parameter becomes finite, and it has been shown that the ^{12}C(3α)+^{16}O configuration has a local energy minimum around the relative distance of 3 fm. In our previous study on ^{28}Si based on the seven-α model, the spin–orbit interaction was not taken into account, and the ground state was a prolate shape with the ^{12}C(3α)+^{16}O configuration[33]. In the present analysis, we find that the spin–orbit interaction plays a big role for the lowering of the pentagon shape, which is oblate.

Furthermore, this method can be extended to *pf* shell nuclei. The α cluster states have been widely discussed in ^{44}Ti and ^{52}Fe, and smooth transition of the wave functions of these nuclei from α cluster states to the lowest *jj*-coupling shell model configurations can be straightforwardly described. Although the effect of α breaking is quite large for the 0^+ state of ^{44}Ti, it is rather limited for the 1^- state. The discovery of negative parity states and inversion doublet structure in the low-lying region of this nucleus were the keys to establishing the concept that the cluster structure is not limited to very light nuclei and is more general. The optimal energy of the 1^- state is obtained around the distance parameter between quasi-clusters and ^{40}Ca of 3.5 fm, and clustering is really important, where the decrease of the energy is limited to about 1 MeV when the breaking of α clusters and the change into quasi-clusters is allowed.

In this article, we applied AQCM to various $4N$ nuclei from ^{4}He to ^{100}Sn, where characteristic magic numbers for the *jj*-coupling shell mode, 28 and 50, which are different from those of the three-dimensional harmonic oscillator, were included. The nuclei corresponding to the subclosure configuration of *j*-upper orbits, 6 (^{12}C), 14 (^{28}Si), 28 (^{56}Ni), and 50 (^{100}Sn), have been successfully described within this model.

Finally, we would like to comment on the tensor interaction, which was omitted in the present analysis. If we switch on the tensor term in the Hamiltonian, the first-order type tensor contribution can be taken into account. We can discuss the attractive or repulsive effect between nucleons in *j*-upper orbits or *j*-lower orbits discussed in Ref. [40] within the present framework. However, to take into account the second-order (two particle–two hole type) tensor, which is much stronger, we need a different model. We have introduced a simplified method in our previous study to take into account this second-order tensor [41], but a more efficient method would be needed.

As future work, we will apply this model to even heavier regions for the purpose of microscopic understanding of α decay. The α cluster is formed in the surface region of the nucleus, but it should be broken inside the surface. In general, shell models underestimate the decay probabilities (because of the small model space for the description of α formation around the surface) and cluster models overestimate (because of the absence of α breaking components). Here, mixing the shell and cluster components is essential to obtain the experimental width [42]. Since our model gives a transparent view of smooth transition, it could simplify the quantitative description of α decay.

Acknowledgements

Numerical calculation was performed at the Yukawa Institute for Theoretical Physics, Kyoto University. This work was supported by JSPS KAKENHI Grant Numbers 716143900002 (N.I.) and 15K17662 (T.S.).

References

[1] P. Maris, J. P. Vary, and A. M. Shirokov, Phys. Rev. C **79**, 014308 (2009).
[2] A. C. Dreyfuss, K. D. Launey, T. Dytrych, J. P. Draayer, and C. Bahri, Phys. Lett. B **727**, 511 (2013).
[3] T. Yoshida, N. Shimizu, T. Abe, and T. Otsuka, J. Phys. Conf. Ser. **569**, 012063 (2014).
[4] W. C. Haxton and C. Johnson, Phys. Rev. Lett. **65**, 1325 (1990).
[5] Y. Suzuki, K. Arai, Y. Ogawa, and K. Varga, Phys. Rev. C **54**, 2073 (1996).
[6] M. Gőppert-Mayer, Phys. Rev. **75**, 1969 (1949).
[7] O. Haxel, J. H. D. Jensen, and H. E. Suess, Phys. Rev. **75**, 1766 (1949).
[8] N. Itagaki, S. Aoyama, S. Okabe, and K. Ikeda, Phys. Rev. C **70**, 054307 (2004).
[9] T. Suhara, N. Itagaki, J. Cseh, and M. Płoszajczak, Phys. Rev. C **87**, 054334 (2013).
[10] T. Suhara and Y. Kanada-En'yo, Phys. Rev. C **91**, 024315 (2015).
[11] J. P. Elliot, Proc. Roy. Soc. A **245**, 128 (1958).
[12] J. P. Elliot, Proc. Roy. Soc. A **245**, 562 (1958).
[13] N. Itagaki, H. Masui, M. Ito, and S. Aoyama, Phys. Rev. C **71**, 064307 (2005).
[14] H. Masui and N. Itagaki, Phys. Rev. C **75**, 054309 (2007).
[15] T. Yoshida, N. Itagaki, and T. Otsuka, Phys. Rev. C **79**, 034308 (2009).
[16] N. Itagaki, J. Cseh, and M. Płoszajczak, Phys. Rev. C **83**, 014302 (2011).
[17] D. M. Brink, Proceedings of the International School of Physics "Enrico Fermi" Course XXXVI, ed. C. Bloch (Academic, New York, 1966), p. 247.
[18] A. B. Volkov, Nucl. Phys. **74**, 33 (1965).
[19] S. Okabe and Y. Abe, Prog. Theor. Phys. **61**, 1049 (1979).
[20] R. Tamagaki, Prog. Theor. Phys. **39**, 91 (1968).
[21] D. J. Marin-Lambarri, R. Bijker, M. Freer, M. Gai, Tz. Kokalova, D. J. Parker, and C. Wheldon, Phys. Rev. Lett. **113**, 012502 (2014).
[22] T. Matsuse, M. Kamimura, and Y. Fukushima, Prog. Theor. Phys. **53**, 706 (1975).
[23] S. Mitsunobu and Y. Torizuka, Phys. Rev. Lett. **28**, 920 (1972).
[24] H. T. Fortune, R. Middleton, and R. R. Betts, Phys. Rev. Lett. **29**, 738 (1972).
[25] H. Horiuchi and K. Ikeda, Prog. Theor. Phys. **40**, 277 (1968).
[26] B. Zhou, Z. Ren, C. Xu, Y. Funaki, T. Yamada, A. Tohsaki, H. Horiuchi, P. Schuck, and G. Röpke, Phys. Rev. C **86**, 014301 (2012).
[27] F. Nemoto, Y. Yamamoto, H. Horiuchi, Y. Suzuki, and K. Ikeda, Prog. Theor. Phys. **54**, 104 (1975).
[28] Y. Fujiwara, H. Horiuchi, and R. Tamagaki, Prog. Theor. Phys. **61**, 1629 (1979).
[29] Y. Fujiwara, Prog. Theor. Phys. **62**, 122 (1979).
[30] Y. Fujiwara, Prog. Theor. Phys. **62**, 138 (1979).
[31] M. M. Hindi, J. H. Thomas, D. C. Radford, and P. D. Parker, Phys. Rev. C **27**, 2902 (1983).
[32] N. Itagaki, A. Ohnishi, and K. Katō, Prog. Theor. Phys. **94**, 1019 (1995).
[33] T. Ichikawa, N. Itagaki, Y. Kanada-En'yo, Tz. Kokalova, and W. von Oertzen, Phys. Rev. C **86**, 031303(R) (2012).
[34] F. Michel, G. Reidemeister, and S. Ohkubo, Phys. Rev. Lett. **57**, 1215 (1986).
[35] T. Wada and H. Horiuchi, Phys. Rev. C **38**, 2063 (1988).
[36] T. Yamaya, K. Katori, M. Fujiwara, S. Kato, S. Ohkubo, Prog. Theor. Phys. Suppl. **123**, 73 (1998).
[37] M. Kimura and H. Horiuchi, Nucl. Phys. A **767**, 58 (2006).
[38] Tz. Kokalova et al., Eur. Phys. J. A **23**, 19 (2005).
[39] Tz. Kokalova, N. Itagaki, W. von Oertzen, and C. Wheldon, Phys. Rev. Lett. **96**, 192502 (2006).
[40] T. Otsuka, T. Suzuki, R. Fujimoto, H. Grawe, and Y. Akaishi, Phys. Rev. Lett. **95**, 232502 (2005).
[41] N. Itagaki, H. Masui, M. Ito, S. Aoyama, and K. Ikeda, Phys. Rev. C **73**, 034310 (2006).
[42] K. Varga, R. G. Lovas, and R. J. Liotta, Nucl. Phys. A **550**, 421 (1992).